COMPARISON OF SOLIDIFICATION SHRINKAGE IN AL-SI ALLOYS A1200 AND A8011 (RECTANGULAR CASTINGS) FROM FINITE ELEMENT MODEL

Supported by tetfund

O. F. Dacosta[1], B. J. Olorunfemi[2]*, A. A. Adekunle[3], S. B. Adejuyigbe[3], S. E. Kayode[4], M. O. Arowolo[3]

[1]Test Development Division, West Africa Examination Council, Corporate Headquarter, Lagos, Nigeria
[2]Department of Mechanical Engineering, Federal University Oye Ekiti, Nigeria
[3]Department of Mechatronics Engineering, Federal University Oye Ekiti, Nigeria
[4]Department of Agricultural & Environmental Engineering, Federal University of Technology, Akure, Nigeria
*Corresponding author: bayode.olorunfemi@fuoye.edu.ng

Received: July 09, 2019 **Accepted:** November 17, 2019

Abstract: Solidification plays a critical role in the production of sound castings. Hence, an understanding of the casting solidification mechanism and how it can be controlled are important considerations in foundry work. Model flow charts were developed for the Gating, Mould Filling and Solidification processes. Finite Element method was used to discretize and solve the governing equations developed for the models using the commercial software, Comsol Multi-Physics. Models developed were validated from experimental data obtained from the Foundry using three different dimensions each for Aluminium alloys A1200 and A8011 by study the temperature profiles and nature of the solidification of the alloys. A comparison of the temperature profiles generated from the experiments and simulations show that in 64% of the processes, there were no significant differences between the experimental and simulated values. However, in comparing the Niyama values obtained from the experiments and those from the simulations, there were no significant differences in 46% of the processes. Threshold Niyama values of 0.103°C-s)$^{1/2}$ /mm for A1200 and 0.143°C-s)$^{1/2}$/mm for A8011 were also established. Below these threshold values, it is predicted that shrinkage will occur in castings from these metals. This research work showed that temperature gradients and cooling rates are important in predicting the occurrence of shrinkage in casting. Also, alloy composition affects the threshold Niyama values. This is because the Niyama value obtained for alloy A8011 (0.143°C-s)$^{1/2}$/mm) was higher than that of alloy A1200 (0.103°C-s)$^{1/2}$/mm) which had a lower silicon content.

Keywords: Finite element, solidification, shrinkage, Al-Si A1200, Al-Si A8011 **c**astings

Introduction

Hsu *et al.* (2006) stated that improving the quality of foundry products has been an issue for research in manufacturing. Numerical models are developed to predict mechanical characteristics and shrinkages porosities. This is done to ensure that casting process and effective parameters are carefully studied for the production of better castings. The mechanism of casting solidification and its control for obtaining sound castings have been a challenge to foundry men (Khanna, 1996). The way a metal solidifies affects its properties. This is because casting develops a metallographic structure which is formed during solidification. Also, the soundness of a casting is dependent on its solidification mechanism and hence a critical factor. Delijusen *et al*. (1986) stated that in recent years, there has been considerable international interest in the development and improvement of near net shape manufacturing methods. In the area of solidification processing, which offers the most direct route to a finished shape, a number of exciting innovations have resulted in the emergence of new casting techniques and foundry procedure.

Consequently, extensive efforts have gone into developing computer models for the numerical simulation of the solidification process. These solidification simulation procedures involve the numerical analysis of heat transfer during solidification using either the finite difference method (FDM) or the finite element method (FEM). According to Droux (1991), knowledge of the location of liquidus and solidus temperatures, the temperature at any point within the casting, local cooling rate, temperature gradient, all at appropriate time interval is of great importance since this information allow for the prediction of the formation of voids, porosity, cracks, micro-segregation and certain microstructures and if necessary to adjust the design of the casting, cooling channels and gates, risers to improve the casting quality.

The structural and mechanical properties of alloys depend on many factors that act during solidification (Nikanorov *et al*., 2005). These include the structure of the melt, the crystallization rate, and the temperature gradient at the liquid-solid interface. According to Skocovsky *et al.* (2009), the mechanical properties of cast Al-Si alloys are significantly affected by eutectic silicon shape in the structure. For this reason, alloys are modified with proper elements.

Shrinkage allowance

Most cast metals shrink or contract volumetrically after solidification and therefore, the pattern to obtain a particular sized casting is made lager by a value which is equivalent to the shrinkage or contraction. The rate of shrinkage varies from one metal to the other because shrinkage is a physical property of metals. Shrinkage also depends on pouring temperature, size that Al-Si binary alloy is an eutectic system with the eutectic composition at 12.6 wt% Si. Silicon reduces the thermal expansion coefficient, increase corrosion and wear resistance. Tavakoli *et al.*, (2009) studied the prediction of shrinkage defects by thermal criterion functions. The study considered the indirect prediction of shrinkage induced solidification defects. It analyzed in the details, the criterion function methods, in particular the Pellini and Niyama criteria. In order to moderate limitations related to the criterion function method, a new method was introduced (Tavakoli *et al.*, 2009; Ziolkowski, 2002) to predict the location of centerline shrinkage in metal castings. The suggested method in the study was derived theoretically based on a heuristic two-scale, macro-meso-scale approach. However, the application of the suggested method was limited to low freezing range alloys. The feasibility of the method was studied by comparing numerical results against the available experimental data. .Hetu *et al.*, (2009) carried out a sensitivity analysis to examine the mould-metal heat transfer coefficient, mould thermal conductivity, wall friction factor, pouring basin temperature and pouring basin head pressure through doing coupled flow simulations on thin-walled castings using the commercial casting simulation software, MAGMASOFT. Validation on a real production casting was performed using the tuned parameters from the verification exercise done to match simulation with reality. Hetu *et al*. (2009) worked on computational methods for mould filling simulation of semi-solid alloys. The work involved a 3-D numerical solution algorithm for the simulation of free surface flow of dense suspensions including particle migration phenomena.

The solution algorithm was validated against flow problems for which experimental and numerical data were available. Pericleous *et al*. (1999) worked on prediction of defects in steel castings with a Multi-physics numerical code while Guleyupoglu *et al.* (1997) studied the modelling of multiphase flow with solidification and chemical reaction in materials processing. The study utilized computational approaches to investigate the multiphase flow and its application in material processes, especially in the areas of directional solidification, pyrolysis and synthesis. It involved the development of an advanced 3-D multi-physics numerical code to model the shape casting process of metals. The work predicted the common defects present in castings and thermal deformation are validated against actual castings. Also, researchers have developed, implemented and tested a casting modelling software tool to simulate filling and residual flow behaviour, solidification behaviour of a range of materials, elasto-visco-plastic behaviour of solid component and its distortion, the formation of macro- and micro-porosity and the impact of feeding shrinkage, and porosity defects of Al-Si Alloy castings made with permanent mould (Wei, 2009; Jain, 2007; Zeid, 2005; Bailey *et al.*, 1997; Mina, 2005).

Materials and Methods

Two varieties of Al-Si alloys were simulated and foundry experiments carried out. Tower Aluminum Rolling Mills, Ota, Ogun State, Nigeria provided the following relevant thermal properties as shown in Table 1.

Table 1: Properties of Alloys A1200 and A8011 been compared together

Type of Alloy	% Composition		Melting Point (^{0}C)	Specific Heat (j/kg.k)	Thermal Conductivity (w/m.k)	Thermal Expansivity (µstrain/ ^{0}c)	D^{4}ensity (kg/m^3)
	Al	Si					
A1200	99.3	0.20	645	893	221	22.8	2680
A8011	98.3	0.47	510	980	81	21.3	2890

Table 2 Dimensions of test pieces and their gating systems (rectangular dimensions)

Sample No	Casting Size (mm)	Down Sprue (mm)	Riser (mm)	Ingate (mm)	Runner Bar (mm)	Vent (mm)
1.	200 × 50 × 39.4	70 × Ø25	70 × Ø25 (2 nos)	24 ×42 × 7 (2 no)	150 × 25 × 20	70 × Ø 5 (2 no)
2.	150 × 50 × 39.4	70 × Ø25	70 × Ø20	30 ×69 × 17 (2 no)		70 × Ø 5 (2 no)
3.	200 × 25 × 19.4	70 × Ø20	70 × Ø10	24 ×42 × 7 (2 no)		70 × Ø 5 (2 no)

Preparation of Test Pieces

Green sand casting was used to produce total number of 6 test samples (3 for each of the two alloys) from two Aluminium alloys A1200 and A8011. Fig. 1 shows alloy A1200 before melting while Fig. 2 shows Aluminium alloy A8011. The castings were carefully produced based on conditions and parameters to facilitate directional solidification. In this experiment, the gating and feeding systems were designed to ensure that the risers solidify later that the hot spots. Also, the necessary shrinkage allowances were taken into consideration in constructing the patterns for the castings (Figs. 1 and 2). Patterns for the rectangular samples are shown in Fig. 3. Table 2 shows the dimensions of test Pieces and their Gating Systems (rectangular dimensions).

Fig. 1: Alloy A1200 plates before melting

Fig. 2: Alloy A8011 plates before melting

Fig. 3: Patterns for the rectangular samples

Mould preaparation

The moulds were prepared from green sand with Bentonite as binder. Properties of the moulding sand include permeability value of 150 cmWH, green strength of 78.4 KN/m^2 and moisture meter of 3.0% (Engineering Materials Dnvelopment Institute, Akure, Nigeria, 2013). Fig. 4 shows a prepared mould for one of the Rectangular shapes.

Fig. 4: Mould for one of the rectangular shapes

Temperature measurement

Two K-type thermocouples probes, 25 mm apart were inserted into each of the moulds. The thermocouples were then connected to digital multi-meters from where temperature readings were taken at 20s intervals with a stop clock. Fig. 5 shows the digital multi-meter and mould/thermocouple arrangement.

Fig. 5: Prepared and coupled mould with thermocouple probes

Fig. 6: Liquid metal being poured into one of the moulds

Melting of the alloy specimens and pouring

The alloy specimens were melted in a diesel fired crucible furnace and the pouring temperatures were read off from an optical pyrometer. Fig. 6 shows the liquid metal being poured into one of the moulds after been melted in a crucible furnace.

Criterion for prediction of shrinkage

In Table 3, Niyama *et al.* (1982) gave existing thermal criteria for prediction of shrinkage as proposed in literatures.

Table 3: Existing thermal criteria for prediction of shrinkage

Criterion	Author	Year Proposed
G	Bishop et al	1951
$\frac{G}{Vs}$	Davies	1975
$\frac{1}{Vsn}$	Khan	1980
$\frac{G}{\sqrt{R}}$	Niyama et al	1982
$\frac{G}{Vs}$	Lacomte- Beckers	1988
$\frac{G0.33}{VS1.67}$	Lee et al	1990
$\frac{G0.38}{VS1.62}$	Kao et al	1994
$\frac{1}{tsmVsn}$	Chiesa	1998

Source: Niyama *et al.* (1982)

Where: G= Temperature Gradient; R= Cooling Rate; V_s= Solidification velocity; t_s = local solidification time

The Niyama criterion which is the most popular and frequently used of all the criteria was adapted for the prediction of shrinkage. It was chosen because it provides a less complex way of predicting shrinkage in castings. The Niyama criterion is given by:

$$\frac{G_j}{\sqrt{R_{ij}}} \quad (1)$$

Where: G is the thermal gradient given by:

$$G_{ij} = (T_j - T_i)/D_s \quad (2)$$

Where: $(T_j - T_i)$ is the difference in temperature between two points *i* and *j* in the casting and Ds is the distance between these points.

R_{ij} the rate of cooling rate from an instant of time τ_1 to τ_2 at a given location inside the casting is given by:

$$R_i = (T_j - T_i)/(\tau_2 - \tau_1) \quad (3)$$

Bailey *et al.*, (1997) stated that if $\frac{G_j}{\sqrt{R_j}}$ is less than 1, then there is a high possibility of shrinkage occurring in Steel castings.

Niyama *et al.*, (1982) investigated steel cylinders of different diameters by casting, and the critical temperature gradient was found to be inversely proportional to the diameter. This observation led to the selection of a new parameter, the temperature gradient divided by the square root of the cooling rate at the end of solidification at each point within a casting. The critical value of the parameter for shrinkage was independent of the alloy and size and shape of castings in the range studied.

The sprue

It was recommended that sprue should be sized to limit the flow rate of molten metal, this is because, the design of the sprue is crucial in order to avoid initiation of turbulent flow in the gating system (Zeid, 2005). The Sprue exit area was calculated from equation. 4

$$A = \frac{G}{W\sqrt{2gh}} \quad (4)$$

Where: A = cross sectional area; G = rate of flow/volume rate; W = specific weight of metal; g = acceleration due to gravity; h = vertical height of molten metal in sprue.

Results and Discussion

Appendices 1-3 show the readings for Alloys A1200 and A8011 of samples 1-3 with dimensions of 200 × 50 × 39.3 mm, 200 × 25 × 19.6 mm and 250 × 25 × 39.3 mm, respectively. While graphs of experimental and simulation results are presented in Fig. 5 – 18.

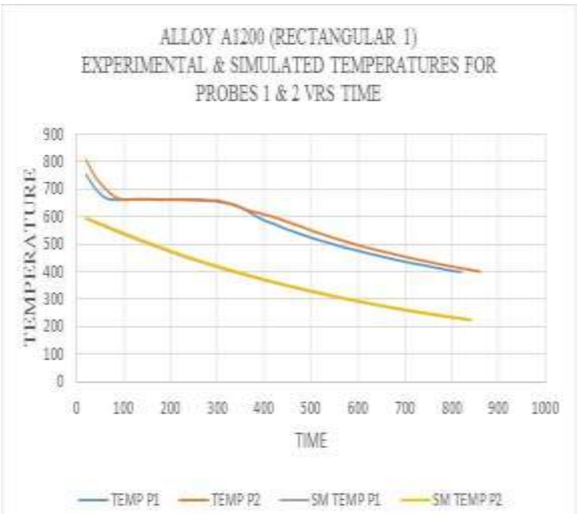

Fig. 7: Probes 1 and 2 Temperature Profile (Experimental and Simulated) Alloy A1200 (Rectangular 1)

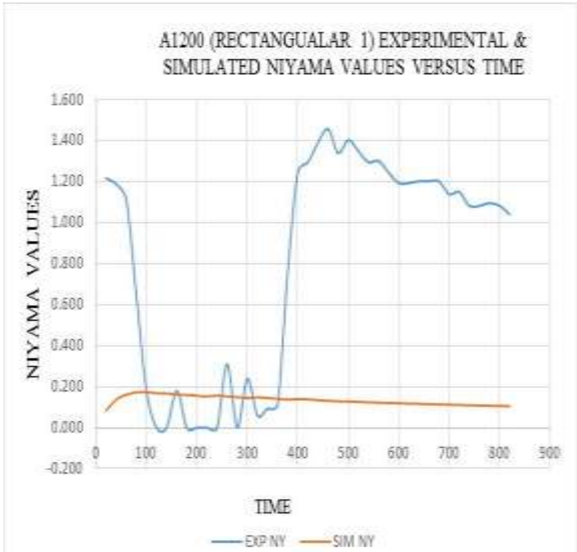

Fig. 8: Graph of experimental and for simulated values of the Niyama Criteria for Alloy A1200 (Rectangular1)

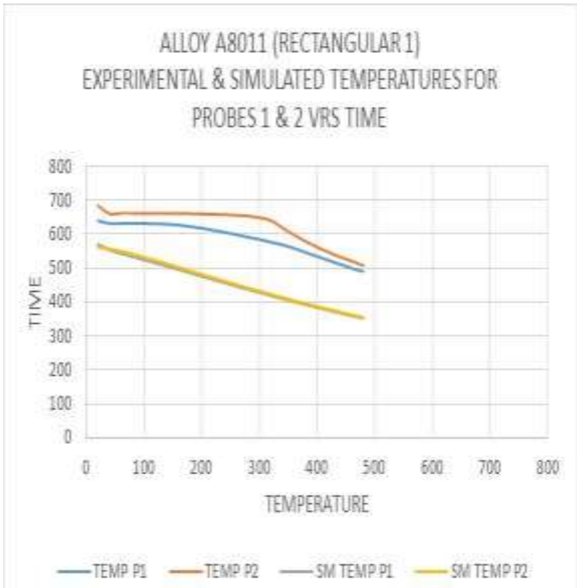

Fig. 9: Probe 1 and 2 temperature profile (experimental and simulated) for Alloy A8011 (Rectangular 1)

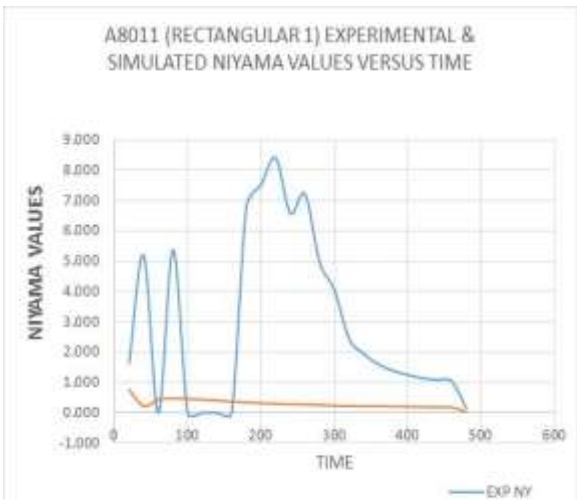

Fig. 10: Experimental and Simulated values of the Niyama Criteria for Alloy A8011 (Rectangular 1)

A look at the profiles of alloy A1200, rectangular 1 as showa that the temperature profiles (Fig. 7) at the two probes are similar in trend. However, the graph of the experimental and simulated Niyama values (Fig. 8) did not show any similar trend. The experimental results peaked at a Niyama value of about 1.4(°C-s)$^{1/2}$ /mm whereas the simulated values are below 0.20(°C-s)$^{1/2}$ /mm. For alloy A 8011, rectangular 1, the temperature profiles (Fig. 9) at the two probes are similar in trend. However, the graph of the experimental and simulated Niyama values (Fig. 10) did not show any similar trend. The experimental results peaked at a Niyama value of about 8.0(°C-s) $^{1/2}$ /mm whereas the simulated values are below 1.0(°C-s) $^{1/2}$ /mm.

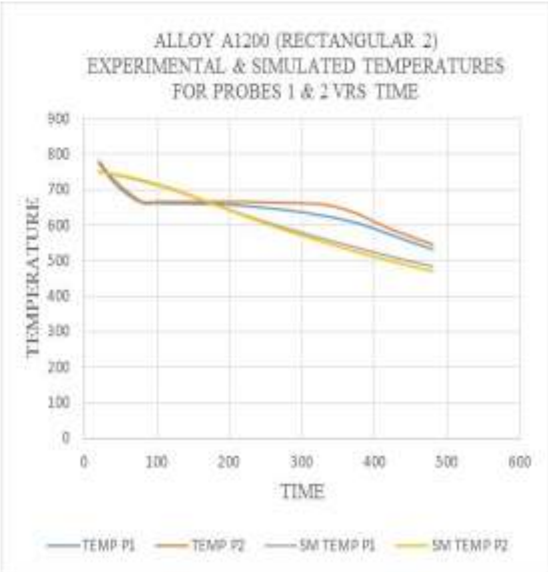

Fig. 11: Probes 1 and 2 temperature profile (experimental and simulated) for Alloy A1200 (Rectangular 2)

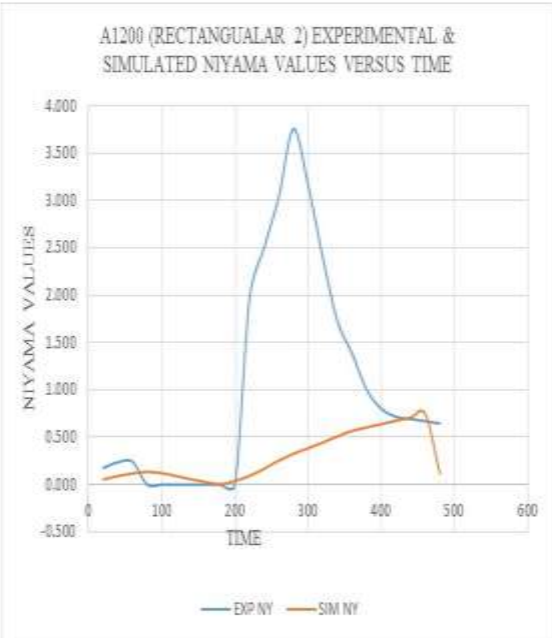

Fig. 12: Graph of Experimental and Simulated values of the Niyama Criteria for Alloy A1200 (Rectangular2)

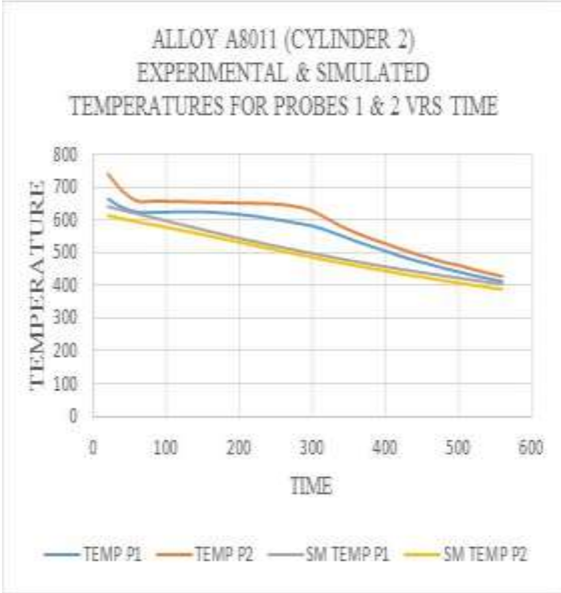

Fig. 13: Probes 1 and 2 TemperatureProfile (Experimental and Simulated) for Alloy A8011 (Rectangular 2

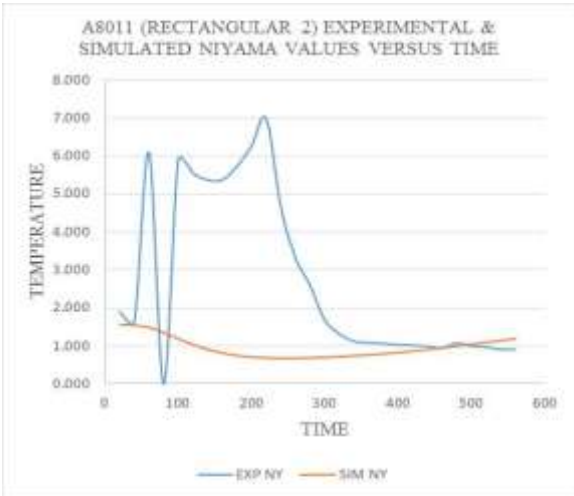

Fig.14: Graph of Experimental and Simulated values of Niyama Criteria for Alloy A8011 (Rectangular 2)

For alloy A1200, Rectangular 2, the temperature profiles (Fig. 11) at the two probes are similar in trend. However, the graph of the experimental and simulated Niyama values (Fig. 12) did not show any similar trend. The experimental results peaked at a Niyama value of about 3.5(°C-s)$^{1/2}$ /mm whereas the simulated values are below 0.50°C-s)$^{1/2}$ /mm. Whereas for alloy A8011 Rectangular 2, the temperature profiles (Fig. 13) at the two probes are similar in trend. However, the graph of the experimental and simulated Niyama values (Fig. 14) do not show any similar trend. The experimental results peaked at a Niyama value of about 7.0 (°C-s)$^{1/2}$ /mm whereas the simulated values are below 1.5(°C-s)$^{1/2}$ /mm.

In the case of alloy A1200, rectangular 3, the temperature profiles (Fig. 15) at the two probes are similar in trend. However, the graph of the experimental and simulated Niyama values (Fig. 16) did not show any similar trend. The experimental results peaked at a Niyama value of about 6.5(°C-s) $^{1/2}$ /mm whereas the simulated values are below 0.50°C-s)$^{1/2}$ /mm. For alloy A 8011, rectangular 3, the temperature profiles (Fig. 17) at the two probes are similar in trend. However, the graph of the experimental and simulated Niyama values (Fig. 18) did not show any similar trend. The experimental results peaked at a Niyama value of about 20.0(°C-s)$^{1/2}$ /mm whereas the simulated values are below 0.5(°C-s)$^{1/2}$ /mm.

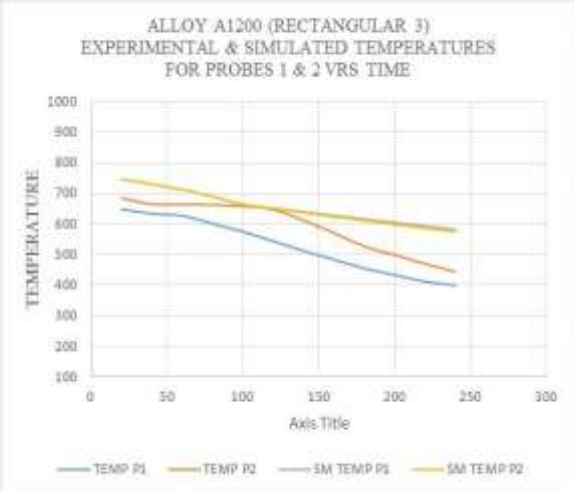

Fig. 15: Probes 1 and 2 Temperature Profile (Experimental and Simulated) for Alloy A1200 (Rectangular 3)

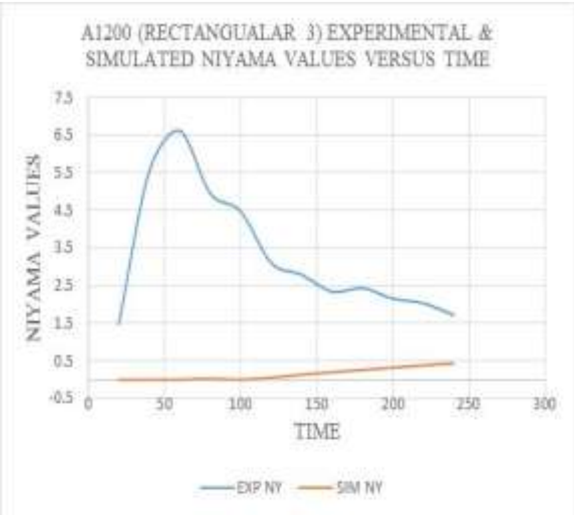

Fig. 16: Graph of Experimental and Simulated values of the Niyama Criteria for Alloy A1200 (Rectangular 3)

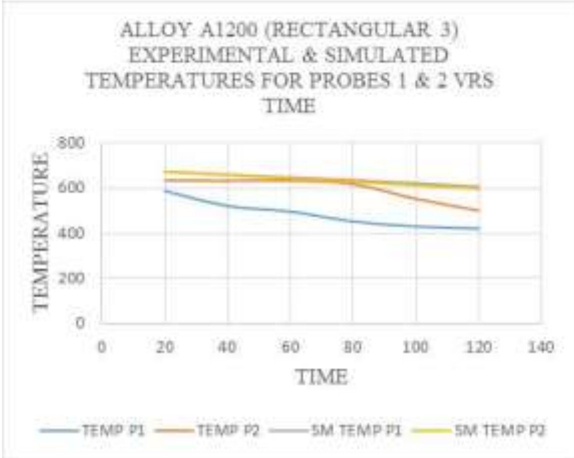

Fig. 17: Probes 1 and 2 Temperature Profile (Experimental and Simulated) for Alloy A8011 (Rectangular 3)

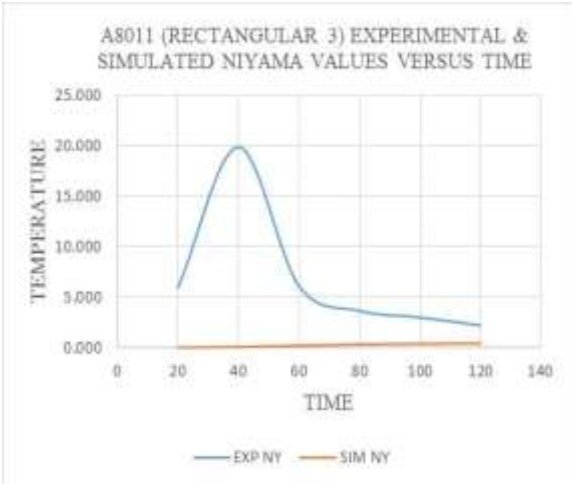

Fig. 18: Experimental and Simulated values of Niyama Criteria for Alloy A8011 (Rectangular 3)

Table 4 gives details of the meshing and discretization used in the simulations. The level of meshing is low and this negatively affected the convergence of the finite elements approximations, it has been stated that, the finer and greater the number of meshing, the better the integrity of the results Bailey *et al.* (1997). This explains the disparity between some of the results of the simulations and experiments simulated mean values.

Table 4: Meshing and discretization data from comsol multi-physics

Alloy	Tetrahedral Elements	Triangular Elements	Meshing Volume	Average Element Quality	Average Growth Rate
A1200 (Rectangular 1)	1619	1086	6.051e-4m^3	0.5584	2.125
A1200 (Rectangular 2)	1231	812	4.171e-4m^3	0.6264	1.842
A1200 (Rectangular 3)	1920	1030	1.365e-4m^3	0.6001	2.071
A8011 (Rectangular 1)	1619	1086	6.051e-4m^3	0.5584	2.125
A8011 (Rectangular 2)	1231	812	4.171e-4m^3	0.6264	1.842
A8011 (Rectangular 3)	1920	1030	1.365e-4m^3	0.6001	2.071

A study of the means of the Niyama values across both Alloys, shapes and sizes indicated that they were lower than the experimental values for both alloys and across the casting sizes. This observation was in agreement with the assertion of Zeid, (2005) who also stated that, unlike physical measurements, casting simulation requires much of user input due to its complexity.

Table 5 Comparison of the means of the Niyama values across Alloys, shapes and sizes

S/No	Casting Size	Mean Of Experimental Niyama Values		Mean of Simulated Niyama Values	
		A1200	A8011	A1200	A8011
1.	200 X 50 X 39.4	0.806	-	0.134	-
2.	150 X 50 X 39.4	1.047	2.728	0.290	0.957
3.	200 X 25 X 19.8	3.307	6.808	0.155	1.605

The Niyama values for both experiments and simulations were higher for Alloy A8011. An explanation for this was supported by Mina (2005) was in the Silicon contents of both alloys, A1200: Al (99.3%) – Si (0.20%) and A8011: Al (98.34%) - Si (0.47%)). The Silicon content was higher in A8011 than A1200.

Conclusion

There has not been an accepted ways of predicting shrinkage in Aluminium alloys. He further stated that since most alloys of aluminium have conductivity more than two times higher than that of Steel, a value of $0.05°C\text{-}s)^{1/2}$ /mm is assumed for Aluminium alloys (Mina, 2005). Carlson *et al.*,(2009) asserted that the Niyama threshold value change from one alloy to the other. He stated a value of $1(°C\text{-}s^{1/2}$ /mm for steel and $0.065(°C\text{-}s)^{1/2}$/mm for the Aluminium-Silicon alloy A8011. From Table 5, the simulated values seem to be much more in consonance with values stated generally for aluminium in the above literature.

This work has therefore been able to determine experimentally and through simulation the threshold Niyama values 0.103 $°C\text{-}s)^{1/2}$ /mm for A1200 and $0.143°(C\text{-}s)^{1/2}$ /mm for A8011. Below these threshold values, it is expected that shrinkage will occur in castings from these metals. With this conclusion, the presence of shrinkage in these alloys can be controlled.

This work highlighted the importance of temperature gradient and cooling rate in predicting the occurrence of shrinkage in a casting. In this work, it was also revealed that alloy composition affects the threshold Niyama values since the values obtained for alloy A8011 were higher than those of alloy A1200. It was also shown that the shapes of the castings did not have significant effect on the Niyama values whereas the smaller sized castings had higher values than the bigger ones.

Conflict of Interest

Authors declare that there is no conflict of interest.

References

Bailey C, Taylor GA, Bounds SM, Moran G & Cross M 1997. PHYSICA: A multi-physics computational framework and its application to casting simulations, International Conference on CFD in Mineral & Metal Processing and Power Generation, CIRO, pp. 419-426.

Carlson KD & Beckermann C 2009. Prediction of shrinkage pore volume fraction using a dimensionless Niyama criterion. *Metallurgical and Materials Transactions*, 40A: 163-175.

Delijusen AJ & Segal AA 1986. Comparison of finite element techniques for solidification problems. *Int. J. Nume. Methods in Engr.*, 23: 1807-1829.

Droux JJ 1991. Three dimensional numerical simulation of solidification by an improved explicit scheme. *J. Computer Methods in Appl. Mech. and Engr.*, 85: 57-74.

Guleyupoglu S 1997. Casting Process Design Guidelines. American Foundrymen's Society (AFS) Transaction, pp. 869-876.

Hetu JF & Ilinca F 2009. Computational Methods for Mould Filling of Semi-Solid Alloys. NRC Publications Archive, Modelling of Casting, Welding and Advanced Solidification Processes, 12(6-7).

Hsu Yeh-Liang & Yu Chia-Chieh 2006. Computer simulation of casting process of aluminium wheels– A case study. *Journal of Engineering Manufacture*, B: 220 - 203.

Khanna OP 1996. A Textbook of Foundry Technology, Published by Dhanpat & Sons, Delhi, India.

Jain N, Carlson KD & Beckermann C 2007. Round Robin Study to assess variations in Casting Simulation Niyama Criterion Predictions. Department of Mechanical and Industrial Engineering, The University of Iowa.

Mina Mi Rin 2005. Research on Porosity Defects of Al-Si Alloy Castings Made With Permanent Mould, pp. 10-70.

Niyama E, Uchida T, Morikawa M & Saito S 1982. A method of shrinkage prediction and its application to steel casting practice. *AFS Cast Metal Res. J.*, 7: 52-63.

Nikanorov SP, Volkov MP, Gurin VN, Burenkov YA, Derkachenko LI, Kardashev B.K, Regel LL & Wilcox WR 2005. Structural and mechanical properties of Al-Si Alloys obtained by fast cooling of a laviated melt. *J. Material Sci. and Engr.*. 390: 63-69.

Pericleous K, Barley C, Cross M, Taylor G, Morgan G & Bounds S 1999. Prediction of Defects in Steel Castings with a Multi-Physics Numerical Code.

Skocovsky P, Tillova E & Belan J 2009. Influence of technological factors on eutectic silicon morphology in Al-Si alloys. *Archive of Foundry Engineering*, 9: 169-172.

Tavakoli R 2009. On the Prediction of Shrinkage Defects by Thermal Criterion Function. Department of Material Science and Engineering, Sharif University of Technology, Teheran, Iran.

Wei J 2009. Modelling of Multiphase Flow with Solidification and Chemical Reaction in Material Processing. A PhD Thesis submitted to the Stony Brook University.

Zeid I 2005. Mastering CAD/CAM. McGraw-Hill Publishers..

Ziolkowski JE 2002. Modelling of an Aerospace Sand Casting Process. M.Sc. degree Thesis submitted to Worcester Polytechnic Institute.

APPENDICES

Appendix 1: Readings for Alloy A1200 and A8011 of sample 1 with 200 × 50 × 39.3 mm Dimensions

Time	Type of Alloy	EXP. Temp. Probe 1 (P1)	EXP. Temp. Probe 2 (P2)	SIM. Temp. Probe 1 (SMP1)	SIM. Temp. Probe 1 (SMP2)	P2-P1	EXP. Thermal Gradient	EXP. Cooling Rate (R)	EXP. $\sqrt{R}$	EXP. Niyama (N)	SMP2 - SMP1	SIM. Thermal Gradient	SIM. Cooling Rate (R)	$\sqrt{R}$	SIM. Niyama
20	Al 1200	753	807	594.26	595.96	54	2.16	3.15	1.775	1.217	1.70	0.068	0.675	0.822	0.083
	Al8011	640	685	570.42	561.75	45	1.80	1.20	1.10	1.64	9.07	0.36	0.22	0.47	0.77
40	Al 1200	702	744	579.62	582.465	42	1.68	2	1.414	1.188	2.84	0.114	0.692	0.832	0.137
	Al8011	632		553.99	57.27	29	1.16	0.05	0.22	5.19	3.28	0.13	0.33	0.58	0.23
60	Al 1200	670	704	565.28	568.625	34	1.36	1.5	1.225	1.110	3.34	0.134	0.695	0.834	0.160
	Al8011	632	662	543.50	50.61	30	1.20	0.00	0.00	0.00	7.11	0.28	0.42	0.64	0.44
80	Al 1200	662	674	551.16	554.725	12	0.48	0.55	0.742	0.647	3.56	0.142	0.682	0.826	0.172
	Al8011	632	662	534.05	42.30	30	1.20	0.05	0.22	5.37	8,24	0.33	0.48	0.69	0.48
100	Al 1200	662	663	537.51	541.075	1	0.04	0.05	0.224	0.179	3.56	0.142	0.671	0.819	0.174
	Al8011	632	661	524.72	32.76	29	1.16	0.00	0.00	0.00	8.04	0.32	0.48	0.69	0.47
120	Al 1200	663	664	524.21	527.655	1	0.04	0	0.000	0.000	3.44	0.138	0.669	0.818	0.168
	Al8011	631	661	515.39	23.23	30	1.20	0.00	0.00	0.00	7.84	0.31	0.51	0.71	0.44
140	Al 1200	663	664	510.95	514.275	1	0.04	0	0.000	0.000	3.32	0.133	0.634	0,796	0.167
	Al8011	630	661	505.76	13.09	31	1.24	0.00	0.00	0.00	7.32	0.29	0.51	0.72	0.41
160	Al 1200	663	664	498.38	501.605	1	0.04	0.05	0.224	0.179	3.22	0.129	0.634	0.796	0.162
	Al8011	627	661	486.31	02.84	34	1.36	0.00	0.00	0.00	6.75	0.27	0.52	0.72	0.38
180	Al 1200	662	663	485.81	488.934	1	0.04	0	0.000	0.000	3.12	0.125	0.617	0.785	0.159
	Al8011	623	661	486.31	92.54	38	1.52	0.05	0.22	0.22	6.23	0.25	0.52	0.72	0.35
200	A1200	662	663	473.57	476.604	1	0.04	0	0.000	0.000	3.03	0.121	0.605	0.778	0.156
	A8011	618	660	476.40	82.17	42	1.68	0.05	0.22	0.22	5.77	0.23	0.52	0.72	0.32
220	A1200	662	663	461.56	464.50	1	0.04	0	0.000	0.000	2.94	0.118	0.597	0.773	0.152
	A8011	612	659	466.50	471.83	47	1.88	0.05	0.22	8.41	5.33	0.21	0.50	0.71	0.30
240	A1200	661	663	449.71	452.56	2	0.08	0	0.000	0.000	2.85	0.114	0.528	0.727	0.157
	A8011	606	658.	456.76	461.84	47.0	2.08	0.10	0.32	6,58	5.09	0.20	0.50	0.71	0.30
260	A1200	660	663	439.22	441,99	3	0.12	0.15	0.387	0.310	2.77	0.111	0.528	0.727	0.153
	A8011	599	656	447.01	451.86	52.0	2.28	0.10	0.32	7.21	4.85	0.19	0.49	0.71	0.29
280	A1200	659	660	428.72	431.42	1	0.04	0	0.000	0.000	2.70	0.108	0.528	0.727	0.149
	A8011	592	654	437.59	442.10	57.0	2.48	0.25	0.50	4.96	4.51	0.18	0.48	0.70	0.28
300	A1200	656	660	418.23	420.85	4	0.16	0.45	0.671	0.239	2.62	0.105	0.528	0.727	0.144
	A8011	585	649	428.32	432.45	62.0	2.56	0.40	0.63	4.05	4.12	0.16	0.48	0.69	0.26
320	A1200	650	651	407.73	410.28	1	0.04	0.45	0.671	0.060	2.55	0.102	0.476	0.690	0.148
	A8011	577	641	419.13	422.94	64.0	2.56	1.10	1.05	2.44	3.82	0.15	0.45	0.69	0.24
340	A1200	640	642	398.28	400.76	2	0.08	0.75	0.866	0.092	2.48	0.099	0.471	0.686	0.145
	A8011	569	619	410.11	413.85	50.0	2.00	1.05	1.02	1.95	3..74	0.15	0.45	0.67	0.23
360	A1200	625	627	388.93	391.35	2	0.08	0.5	0,707	0.113	2.42	0.097	0.471	0.686	0.141
	A8011	559	598	401.09	404.75	39.0	1.56	0.95	0.97	1.60	3.66	0.15	0.43	0.66	0.22
380	A1200	605	617	379.59	381.94	12	0.48	0.4	0.632	0.759	2.35	0.094	0.471	0.686	0.137
	A8011	547	579	392.59	396.08	32.0	1.28	0.85	0.92	1.39	3.49	0.14	0.43	0.66	0.21
400	A1200	587	609	370.25	372.53	22	0.88	0.5	0.707	1.245	2.28	0.091	0.431	0.657	0.139
	A8011	535	562	384.18	387.48	27.0	1.08	0.75	0.87	1.25	3.30	0.13	0.42	0.65	0.20
420	A1200	575	554	361.68	363.90	24	0.96	0.55	0.742	1.294	2.22	0.089	0.414	0.644	0.138
	A8011	523	547	375.96	379.09	24.0	0.96	0.70	0.84	1.15	3.13	0.13	0.41	0.64	0.20
440	A1200	560	560	353.46	355.62	28	1.12	0.65	0.806	1.389	2.16	0.086	0.414	0.644	0.134
	A8011	512	533	367.98	370.96	21.0	0.84	0.60	0.77	1.08	2.99	0.11	0.40	0.64	0.19
460	A1200	548	548	345.23	347.33	27	1.08	0.55	0.742	1.456	2.10	0.084	0.414	0.644	0.131
	A8011	500	521	360.47	362.86	21.0	0.84	0.65	0.81	1.04	2.85	0.11	0.38	0.62	0.18

Appendix 2: Readings for Alloy A1200 and A8011 of sample with 200 × 25 × 19.6 mm dimension

Time (sec)	Type of Alloy	Exp. Temp Probe 1 (P1)	Exp. Temp Probe 2 (P1)	Simulated Temp P1(SmP1)	Simulated Temp P2 (SmP2)	P2-P1	Exp. Thermal Gradient	Exp. Cooling Rate (R)	EXP= √R	Ex. Niyama (N)	Sim. P2 – Sim. P1	Sim Thermal Gradient	Sim. Cooling Rate	Sim. EXP= √R	Sim. Niyama
20	A1200	774	781	750.83	751.68	7	0.28	2.55	1.597	0.175	0.82	0.033	0.366	0.605	0.054
	A8011	664	741	640.96	613.57	77	3.08								
40	A1200	722	730	742.91	744.32	8	0.32	1.85	1.36	0.235	1.41	0.056	0.392	0.526	0.090
	A8011	638	688	603.74		50	2.00								
60	A1200	686	693	734.44	736.48	7	0.28	1.35	1.162	0.241	2.04	0.081	0.476	0.682	0.118
	A8011	624	658	594.75		34	1.36								
80	A1200	663	666	724.45	725.91	3	0.12	0.00	0.00	0.00	2.45	0.098	0.548	0.740	0.131
	A8011	623	657	586.25		34	1.36								
100	A1200	662	666	713.56	715.96	4	0.16	0.00	0.00	0.00	2.39	0.096	0.629	0.793	0.121
	A8011	624	657	577.77		33	1.32								
120	A1200	661	566	701.49	703.37	5	0.2	0.00	0.00	0.00	1.88	0.075	0.712	0.844	0.089
	A8011	625	656	569.04		31	1.24								

Appendix 3: Readings for Alloy A1200 and A8011 of sample with 250 × 25 × 39.3 mm dimension

Time (sec)	Type of Alloy	Exp. Temp Probe 1 (P1)	Exp. Temp Probe 2 (P1)	Simulated Temp P1(SmP1	Simulated Temp P2 (SmP2)	P2-P1	Exp. Thermal Gradient	Exp. Cooling Rate(R)	EXP= √R	Ex. Niyama (N)	Sim. P2 – Sim. P1	Sim Thermal Gradient	Sim. Cooling Rate	Sim. EXP= √R	Sim. Niyama
20	A1200	648	685	746.37	746.16	17	1.48	1.00	1.00	1.48	0.19	0.008	0.777	0.881	0.009
	A8011	587	534	671.71	671.84	47	1.880	0.10	0.316	5.945	0.89	0.095	0.742	0.862	0.041
40	A1200	534	685	730.61	730.64	31	1.24	0.05	0.22	5.545	0.03	0.001	0.916	0.957	0,001
	A8011	521	632	699.14	656.99	111	4.44	0.05	0.224	19.856	2.15	0.086	0.743	0.862	0.100
60	A1200	627	654	712.10	712.32	37	1.48	0.05	0.22	6.619	0.23	0.009	1.099	1.049	0.005
	A8011	496	633	647.15	642.14	137	5.48	0.80	0.894	6.127	5.01	0.200	0.752	0.867	0.231
80	A1200	601	663	689.51	690.33	52	2.48	0.25	0.50	4.96	0.83	0.033	1.315	1.147	1.025
	A8011	452	617	684.83	627.09	165	6.50	3.25	1.803	3.661	7.74	0.310	0.769	0.877	0.353
100	A1200	575	658	663.91	664.03	83	3.32	0.55	0.74	4.477	0.12	0.005	0.682	0.825	0.006
	A8011	430	552	612.08	611.70	122	4.88	2.60	1.612	3.025	3.37	0.375	0.803	0.895	0.418
120	A1200	544	647	651.57	650.39	103	4.12	1.75	1.32`	3.114	1.18	0.047	0.676	0.872	0.058
	A8011	421	500	606.23	595.55	79	3.16	2.00	1.414	2.234	10.58	0.423	0,841	0.917	0.452